Experimental and ab initio Investigation on the Effect of CO and CO 2 during Hydrodeoxygenation of m-Cresol over Co/SBA-15

Camila Teles, Saber Gueddida, Roger Deplazes, Carmen Ciotonea, Nadia Canilho, Sébastien Lebègue, Jérémy Dhainaut, Michael Badawi, Frédéric Richard, Sébastien Royer

ChemCatChem

Research Article
doi.org/10.1002/cctc.202201327

Chemistry Europe
European Chemical Societies Publishing

www.chemcatchem.org

Special Collection

Experimental and *ab initio* Investigation on the Effect of CO and CO_2 during Hydrodeoxygenation of m-Cresol over Co/SBA-15

Camila A. Teles,[a] Saber Gueddida,[b] Roger Deplazes,[c] Carmen Ciotonea,[d] Nadia Canilho,[e] Sébastien Lebègue,[b] Jérémy Dhainaut,[c] Michael Badawi,[b] Frédéric Richard,*[a] and Sébastien Royer*[c]

The hydrodeoxygenation (HDO) is a fundamental step in the production of biofuels from lignin, and the catalyst type and reaction conditions can play an important role. In this work, Co nanoparticles finely dispersed in the porosity of SBA-15 stand out a high selectivity toward deoxygenated products (63% of methylcyclohexenes and 16% of methylcyclohexane) in the HDO of m-cresol (30 bar of pressure, temperature of 350 °C). The effect of co-feeding CO and CO_2, which can be present in the pyrolysis gas after transformation of carboxylic acids, was investigated. An unexpected positive effect on the stability of the catalyst was observed when CO_2 was added in the feed stream. On the contrary, the presence of CO led to a strong decrease of the m-cresol conversion. These experimental findings are supported by DFT calculations which show that the m-cresol is much more strongly adsorbed than CO_2 at the Co@SiO_2 interface while the interaction energy of CO is close to the one of m-cresol.

Introduction

Depletion of fossil fuels and the increasing environmental concerns related to their uses, stimulate the development of renewable alternative energies. In this line, lignocellulosic biomass is viewed as an abundant and renewable source that can be converted to green platform chemicals and biofuels to alleviate the dependence to fossil fuels. Lignin, which represents 15–30% of the lignocellulose, is currently poorly valorized and serves as combustible for the pulp and paper industry. Considering the aromatic nature of this biopolymer, lignin could be transformed into a liquid bio-oil applying a pyrolysis process.[1] However, the bio-oil obtained is far to meet the requirements needed for a use in modern engines due to its corrosivity, chemical instability, and viscosity. Then, its upgrading is required, notably to transform the oxygenated compounds into alkanes and aromatics-type molecules reaching a bio-oil with more appropriate physical characteristics.[2]

The catalytic hydrodeoxygenation (HDO) process is one of the most effective ways to remove the oxygenated compounds from the bio-oil.[3] Over the past few years, detailed investigations on HDO reaction have been reported, including the effect of catalyst composition, reaction parameters and elucidation of reaction mechanism by using model molecules mimicking the lignin pyrolysis vapors (such as phenol, cresols and guaiacol). Both, theoretical and experimental studies showed that the transformation of phenolic compounds such as m-cresol involves two main reaction routes: (i) direct deoxygenation (DDO) either by direct cleavage of the C–O bond or by involving a tautomer intermediate yielding toluene as a final product; (ii) hydrogenation (HYD) of the aromatic ring yielding methylcyclohexanone and methylcyclohexanol followed by dehydration to produce methylcyclohexenes or C–O bond cleavage to directly produce methylcyclohexane.[4] The nature of the active phase may control the reactant adsorption and orientate the selectivity, and then has a key role in determining the reaction pathway. Noble metals such as Pt, Pd and Rh are particularly efficient in hydrogenation steps. When they are combined with a second oxophilic metal such as Ru, Re and Mo, or if supported on oxophilic materials such as ZrO_2, TiO_2 and Nb_2O_5, DDO route is promoted.[4c,5] However, noble metals

[a] Dr. C. A. Teles, Dr. F. Richard
Institut de Chimie des Milieux et Matériaux de Poitiers, CNRS UMR 7285
Université de Poitiers
Rue Michel Brunet
BP633, 86022 Poitiers (France)
E-mail: frederic.richard@univ-poitiers.fr
[b] Dr. S. Gueddida, Dr. S. Lebègue, Dr. M. Badawi
Laboratoire de Physique et Chimie Théoriques, CNRS UMR 7019
Université de Lorraine
Vandœuvre-lès-Nancy
54506 Nancy (France)
[c] R. Deplazes, Dr. J. Dhainaut, Dr. S. Royer
Unité de Catalyse et Chimie du Solide, CNRS UMR 8181
Université de Lille, Centrale Lille, Université d'Artois
F-59000 Lille (France)
E-mail: sebastien.royer@univ-lille.fr
[d] Dr. C. Ciotonea
Unité de Chimie Environnementale et Intéractions sur le Vivant, UR4492, SFR Condorcet CNRS 3417
Université du Littoral Côte d'Opale
59140 Dunkerque (France)
[e] Dr. N. Canilho
L2CM, CNRS UMR 7053
Université de Lorraine
Vandœuvre-lès-Nancy
54506 Nancy (France)

Supporting information for this article is available on the WWW under https://doi.org/10.1002/cctc.202201327

Special Collection *This publication is part of a Special Collection on "French Conference on Catalysis 2022". Please check the ChemCatChem homepage for more articles in the collection.*

are expensive and scarce, thus their replacement with transition metals, especially for large scale catalysis, would be preferable. In this line, Ni favors the formation of hydrogenated products while Co and Fe present interesting selectivities to deoxygenated products.[6] However, such metals usually present a lower activity, which can be overcome by different strategies such as tuning the metal particle size. For example, Yang et al.[7] showed that the activity and selectivity toward the DDO route of a Ni/SiO_2 catalyst can be significantly enhanced by decreasing Ni particle size.

In the HDO process, the reaction parameters, such as reaction temperature, hydrogen pressure or feedstock composition may also orientate the reaction route. For instance, high H_2 pressures and low temperatures favor the hydrogenation route, while the DDO route is favored at atmospheric pressure or high temperatures.[5c,8] The effect of gas composition is however rarely studied, while lignin pyrolysis vapors may contain gases such as CO and CO_2 originating from the conversion of esters and carboxylic acids.[9] The effect of CO in the HDO reaction of phenolic compounds was reported over sulfided catalysts[10] and over Fe/SiO_2.[11] When the HDO of 2-ethylphenol over $CoMo/Al_2O_3$ and $NiMo/Al_2O_3$ catalysts was carried out in the presence of CO, a strong inhibition was found over $CoMo/Al_2O_3$ catalyst while a limited effect was observed for $NiMo/Al_2O_3$.[10] The inhibitor effect of CO was explained by its competitive adsorption with the phenolic compound. The difference observed among the catalysts was attributed to the difference of CO adsorption energy over Co and Ni surfaces.[11] Olcese et al.[12] studied the effect of CO and CO_2 in the HDO reaction of guaiacol over a Fe/SiO_2 catalyst. While CO_2 showed a positive effect on guaiacol conversion, CO had a strongly negative effect due to the carburization of iron and formation of coke, thus causing catalyst deactivation.

By using theoretical approaches, Gueddida et al.[13] investigated the interaction mode of phenolic compounds such as phenol, anisole, catechol and guaiacol as well as the inhibiting effect of CO and H_2O over various metallic clusters (Ni, Co, Fe and Cu) supported on silica. The calculated adsorption energies of the phenolic compounds suggest that their interaction was stronger over Ni, followed by Co, Fe, and then Cu. By comparison with the adsorption energies of CO, the authors concluded that the inhibiting effect of CO on the oxygenated compounds adsorption should be negligible for Ni, Co and Fe supported on silica, while it becomes significant for Cu.

In the present paper, the effect of CO and CO_2 gases on the m-cresol HDO in gas phase was investigated. Considering the conditions applied for fast pyrolysis of biomass process, and with the objective to couple pyrolysis and post-HDO treatment without condensation of bio-oil vapors, reaction conditions selected for the study were 350 °C and 30 bars as H_2 pressure. The selected catalyst was a SBA-15 supporting Co nanoparticles (NPs). The catalytic activity of the catalyst was discussed on the basis of DFT calculations which allowed to estimate the adsorption energies of m-cresol as well as CO and CO_2 over the Co metal clusters and Co-silica interface. Thus, the understanding of the impact of various gas composition can help in the design of more active and stable catalysts for the upgrading process of lignin-based bio-oil.

Results and Discussion

Catalyst properties

The use of the melt-infiltration method to disperse transition metals over a SBA-15 support presents the advantage to retain its high surface area without alteration of the ordered mesopores structure. After activation, mesopore confined NPs are obtained. More than this, the preparation method allows to adjust the localization and the size of the transition metal oxide (TMO) by changing some of the synthesis parameters, such as the time of the infiltration process.[14]

Nitrogen physisorption analysis was used to evaluate the textural properties of the Co/SBA material. The shape of adsorption/desorption isotherm (Figure S1) of the bare SBA-15 support, and especially its H1 hysteresis loop, did not change after Co infiltration, showing that its pore structure was preserved. Textural properties are summarized in Table 1. A notable decrease in surface area following the reduction of Co (from 801 to 431 $m^2 g^{-1}$) is measured. This decrease is associated to a partial blockage of pores by mesopore confined cobalt particles. The average pore sizes, as evaluated by applying the B.J.H. model on the desorption branches, are 7.2 and 6.5 nm for the support and reduced Co/SBA samples, respectively.

After thermal activation, highly dispersed cobalt oxide or phyllosilicate phase are expected to form. Indeed, the DRX pattern of calcined CoO_x/SBA does not show any clear diffraction peak (Figure 1a). H_2-TPR experiment shows that cobalt oxide phase reduction took place at very high temperature (peak centered at 874 °C, Figure 1b), suggesting that Co is in strong interaction with the silica support. Such high

Table 1. Textural and physicochemical properties of the Co/SBA catalyst.

Catalyst	Textural properties[a] S [$m^2 g^{-1}$]	V_p [$cm^3 g^{-1}$]	d_p [nm]	d[b] [nm]	H_2 uptake [mmol g^{-1}] Exp.[c]	Cal.[d]	Metal reducibility [%]	Lewis Acidity[e] [μmol g^{-1}]
Co/SBA	431 (801)	0.76 (1.03)	6.5 (7.2)	5.5 (6.1)	1.6	2.3	72	20

[a] Surface area determined by nitrogen physisorption analysis - in parentheses data referring to the bare support; [b] metal particle size estimated by STEM images - in parentheses, average particle size calculated from XRD (reduced sample); [c] Quantity of hydrogen determined by the H_2-TPR experiments; [d] Theoretical quantity of H_2 calculated according to the Co catalyst loading, calculated to completely reduce Co(+III) to Co(0); [e] Acidity measured by DRIFTS of pyridine adsorbed.

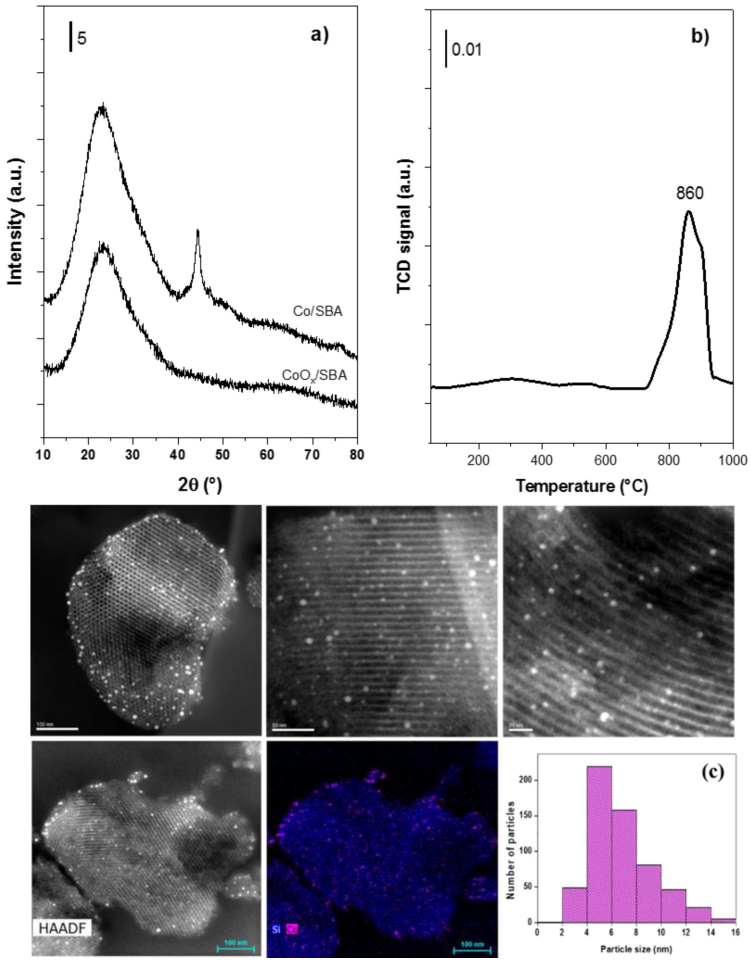

Figure 1. a) X-ray diffraction for the calcined (CoOx/SBA) and reduced (Co/SBA) catalyst; b) H_2-TPR profile; c) representative HAADF images of reduced Co/SBA catalyst and the respective histogram of Co particle sizes (580 particles).

reduction temperature is typical for the reduction of ionic cobalt from Co–O–Si phases, as in phyllosilicate phase.[15] Additionally, a broad and weak hydrogen consumption is observed at temperatures of 350 °C–550 °C, that can be ascribed to the reduction of Co_3O_4 NPs.[15] The XRD pattern collected for the sample reduced at 800 °C display a sharp reflection at $2\theta = 44.5°$ which is associated to Co^0 phase (ICDD n° 05–0727). The presence of this peak suggests the reduction, at least partial, of cobalt oxide NPs into metallic Co^0.

Metallic Co NP sizes and dispersion over the support was evaluated by electronic microscopy. A selection of representative HAADF images (Figure 1c and S2) is presented. First of all, well-ordered arrays of mesopores are observed throughout the support, suggesting that the MI process does not affect the silica structure. The images show the Co^0 NPs homogenously dispersed onto the porosity with very few small particles localized at the external surface of silica. The average Co^0 NPs size obtained by microscopy was of 5.5 nm, close to the value calculated from the XRD pattern of the reduced catalyst by applying the Scherrer equation after Warren's correction for instrumental broadening (6.1 nm, Table 1). This average size is comparable to the pore size of the support (6.5 nm), confirming the physical confinement occurring for the $Co(O_x)$ particles in the support mesopores, after the thermal treatments.

The type and density of acid sites present on the catalyst were determined by DRIFTS of adsorbed pyridine (Figure S3, Table 1). Adsorption bands at ~1450 and ~1610 cm^{-1} can be ascribed to the vibration modes of pyridine adsorbed on Lewis acid sites. Both bands disappear at 250 °C indicating that acid sites are of weak strength. Moreover, the density of acid sites was estimated to be 20 $\mu mol\,g^{-1}$. Such low acidity is attributed to the presence of residual unreduced surface Co(+II/+III) species, in line with a reduction degree of 72% as evaluated by H_2-TPR (Table 1).

Catalyst properties

The catalytic performance of the Co/SBA catalyst was measured in the HDO of m-cresol in gas phase (350 °C and 30 bar of total pressure). Figure 2a shows the product distribution obtained at low level of m-cresol conversion (12%). Deoxygenated compounds such as methylcyclohexenes isomers

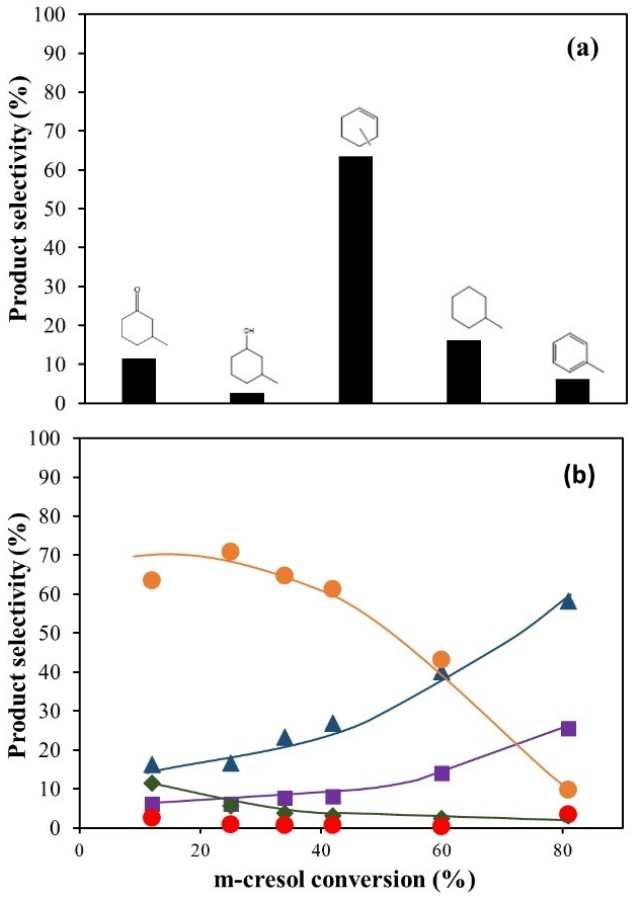

Figure 2. (a) Product distribution obtained in the HDO of m-cresol at 12% of conversion; (b) product selectivity as a function of m-cresol conversion. (▲) methylcyclohexane; (●) methylcyclohexenes; (■) Toluene, (◆) 3-methylcyclohexanone; (●) 3-methylcyclohexanol.

(3,4-methylcyclohexene and 1-methylcyclohexene) accounting for 63 mol%, and methylcyclohexane accounting for 16 mol%, were the main products obtained. Minor formations of toluene (6 mol%) and oxygenated products (3-methylcyclohexanone: 11 mol% and 3-methylcyclohexanol: 3 mol%) are observed. This result indicates the high deoxygenation capacity of cobalt-based catalysts. The formation of such products can be explained by two main reaction pathways:

(i) the direct deoxygenation (DDO route) leading to toluene, either by the direct cleavage of the C–O bond or by involving the formation of a tautomer intermediate (3-methyl-3,5-cyclohexadienol) with further hydrogenation of its carbonyl group;

(ii) the hydrogenation (HYD route) in which the aromatic ring is first hydrogenated yielding 3-methylcyclohexanone and 3-methylcyclohexanol with further dehydration to produce methylcyclohexenes and final hydrogenation to methylcyclohexane. Direct cleavage of 3-methylcyclohexanol to methylcyclohexane can also be considered.[6d,16] The hydrogenation route also involves the passage through the tautomer intermediate (3-methyl-3,5-cyclohexadienol) which can be considered as a common intermediate of both DDO and HYD routes.

The preference toward a reaction pathway is strongly dependent on the type of metal. Metals such as Pt, Pd, Rh or Ni usually promotes the hydrogenation route leading to ketone and alcohol as main products if these metals are supported on inert support such as silica. Alkenes and alkanes are produced if these last metals are supported on acidic materials.[5a,17,18] The use of oxophilic metals or supports to establish a stronger affinity between oxygen atom from the oxygenated organics and the catalyst surface is expected to favor the DDO route, leading to improved yields to toluene.[4c,5c–f,19]

The effect of conversion on the product selectivity is showed in Figure 2b. As the conversion increases, selectivity to toluene and m-cyclohexane increases while selectivity to m-cyclohexenes and m-cyclohexanone continuously decreases. This evolution confirms the existence of the two parallel routes occurring for the HDO of m-cresol over Co/SBA-15 catalyst: DDO yielding toluene, and HYD yielding mainly m-cyclohexenes and m-cyclohexane. Our results are in accordance with earlier reports for the HDO of m-cresol over Co and Ni when reaction was conducted at comparable experimental conditions.[6d,20] Then, the higher selectivity to hydrogenated products (methylcyclohexenes and methylcyclohexane) indicates that the HYD route is favored. In order to conclude on the toluene reactivity under these experimental conditions, an additional experiment was performed using a model feed containing both m-cresol and toluene. No toluene conversion was observed, indicating that toluene hydrogenation into m-cyclohexene or m-cyclohexane did not occur in these conditions. In order to unveil the way of m-cyclohexenes and m-cyclohexane formation, reaction was also performed using a model feed containing m-cresol and m-cyclohexanol. Complete conversion of the alcohol was observed yielding a mixture of the m-cyclohexenes isomers. Thus, the presence of weak acid sites observed on the catalyst (Table 1) is enough to catalyze the dehydration of 3-methylcyclohexanol into m-cyclohexenes, which can be further hydrogenated to methylcyclohexane. However, direct cleavage of the C–O bond of m-cyclohexanol to m-cyclohexane cannot be completely excluded.

In order to verify the advantage of using SBA-15 to disperse the Co metallic phase, an experiment was performed using a 10 wt.% Co supported on commercial silica (Co/SiO_2) exhibiting higher Co particle size: 5.5 nm and 32 nm for Co/SBA and Co/SiO_2, respectively. As expected, the former is about 7 times more active that the latter due to the presence of small metal particle size (Table 2). This significant difference in activity also confirms that the Co particles located at the external surface of the SBA-15 grains will contribute a few to the activity of the Co/SBA catalyst and that the particles located inside the channel-type pores, even of size a few bellow the pore size, are accessible to the reactant. Both catalysts showed a high selectivity to deoxygenated products (Table S1, ESI). Larger Co-nanoparticles favor both the fully deoxygenation of m-cresol (97 mol% of deoxygenated products over Co/SiO_2 versus 86 mol% over Co/SBA) and the hydrogenation of alkenes into alkane. However, as indicated above, the use of catalyst

Table 2. Calculated reaction rates for the transformation of m-cresol over different supported catalysts after 1 h on stream.

Catalyst	Temperature [°C]	Pressure [bar]	r[a] [mmol g_{metal}^{-1} h^{-1}]			REF
			r_{TOT}	r_{DDO}	r_{HYD}	
Co/SBA	350	30	520	152	368	This work
Co/SiO_2	350	30	72	15	57	This work
Co/Al_2O_3	340	40	57	3	54	[6d]
Pd/SiO_2	300	30	245	5	240	[22]

[a] Calculated reaction rates for m-cresol conversion (TOT), direct deoxygenation (DDO) and hydrogenation (HYD) pathways for the transformation of m-cresol.

exhibiting small nanoparticle sizes (5.5 nm for Co/SBA) allows to increase the deoxygenation rate in a large extend. A comparison was also made for different catalysts tested at close experimental conditions. When activity was normalized per gram of active element, the Co/SBA presented in this work was 9-fold more active than a Co/Al_2O_3 catalyst, even considering that both catalysts present close Co particle size (6.1 and 6.5 nm, respectively). It also suggests the beneficial effect of using SBA-15 as a support to confine cobalt nanoparticles. Also, Co/SBA was 2-fold more active that Pd supported catalyst (Pd/SiO_2) besides being significantly more active to the formation of deoxygenated products. In this case, the Pd-based catalyst present a larger particle size (9 nm), however, previous study demonstrated that Pd particle size does not affect the product selectivity.[21] In conclusion, the results obtained demonstrate that supported cobalt NPs on SBA-15 can be considered as an active catalyst for the HDO process.

The effect of co-feeding of CO and CO_2 on the reactivity of m-cresol was herein evaluated by following m-cresol conversion as a function of time on stream (TOS), starting at ~90% of m-cresol conversion (Figure 3). When the m-cresol HDO is conducted under pure H_2, the conversion decreases with time on stream (TOS). Such observed evolution characterizes a rapid deactivation of the Co/SBA catalyst. Interestingly, the addition of CO_2 at 24 kPa after 3 hours on stream helps in the stabilization of the catalyst activity. After 7 hours on stream, m-cresol conversion is close to 50% when reaction is conducted in the presence of CO_2, while it stabilizes at 27% under pure H_2. This result suggests that the presence of CO_2 slows down the catalyst deactivation. On the contrary, a strong decrease in m-cresol conversion is observed when adding CO to the H_2 feed. Once the flow of CO is stopped, the conversion of m-cresol stayed at a very low level, indicating that the presence of CO leads to an irreversible deactivation of Co/SBA catalyst, on the contrary to the presence of CO_2 that helped to the stabilization of the catalyst activity at a level higher than under pure H_2.

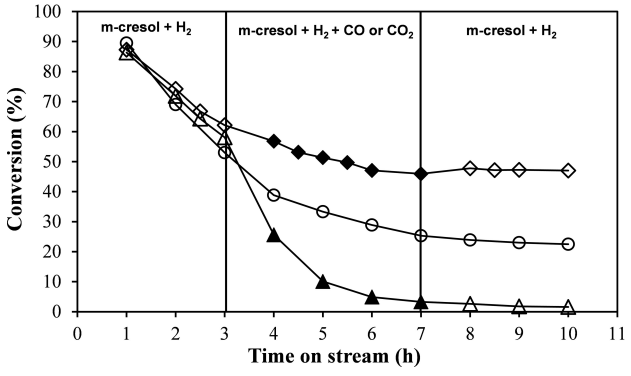

Figure 3. Conversion of m-cresol at 350 °C and 30 bar of total pressure, in the presence of only H_2 (**O**, Δ, ◇); H_2+CO_2 (◆) and H_2+CO (▲). Empty symbols represent conversion obtained with the gas flow composed of only H_2 in addition to m-cresol, in the first and last 3 hours of reaction. Filled symbols represent conversion in the presence of CO_2 (24 kPa) or CO (24 kPa) added to the gas phase.

In order to follow the effect of both CO and CO_2 on the reaction product distribution, the evolution of products yield was monitored with TOS (Figure 4). For all experiments, in the presence of only H_2 (Figure 4a) or in the presence of CO_2 (Figure 4b) and CO (Figure 4c), the yields measured during the first 3 hours of reaction are obtained under the same experimental conditions, hence comparable results are obtained. An increase in the yield of methylcyclohexenes is observed, while the yield of toluene and methylcyclohexane decrease. Methylcyclohexanone and methylcyclohexanol yields remain almost constant, at a level below 10%. These results indicate that the active sites responsible for the DDO and hydrogenation of methylcyclohexenes into methylcyclohexane are rapidly deactivated. When the whole reaction takes place without CO and CO_2 (Figure 3a), the yield to methylcyclohexenes stabilizes around 15 mol% while the yields of all other products stabilize below 4 mol%. From these observations, we can propose that the active sites for the C–O bond scission and the hydrogenation of alkenes into methylcyclohexane are the first sites to deactivate while those responsible for the alkenes production by hydrogenation of aromatic ring followed by dehydration of alcohol remain still active. This is in line with other studies that have demonstrated that the active sites responsible for the DDO route are rapidly deactivated in the beginning of reaction.[5f,23]

When the experiments are performed in the presence of CO_2, from 3 to 7 hours on stream, analysis of the gas effluent indicated the formation of CH_4 and CO, as CO_2 hydrogenation products (Figure 5). CH_4 is produced from CO_2 and H_2 according the Sabatier reaction while CO can form by the reverse water gas shift reaction. However, the conversion of CO_2 remains relatively low (~20%). When reaction is conducted in the presence of CO, CO is no more detected in the gas phase under our experimental conditions. The absence of CO in the reaction feed suggest the strong affinity of this molecule with surface sites of the catalyst. Also, considering the very low content of CO in the feed stream (0.8%) CO may remain adsorbed on the

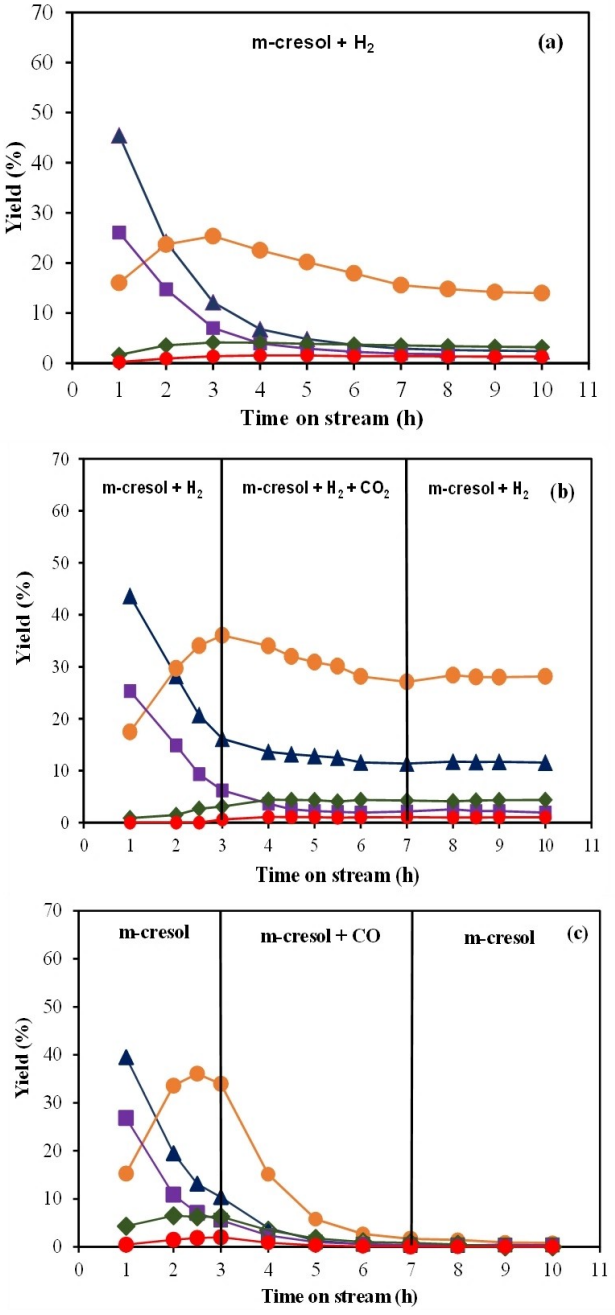

Figure 4. Yield of the products obtained in the reaction performed under: (a) only H_2; (b) in the presence of 24 kPa of CO_2 and (c) in the presence of 24 KPa of CO (350 °C, 30 bar). (▲) methylcyclohexane; (●) methylcyclohexenes; (■) Toluene, (◆) 3-methylcyclohexanone; (●) 3-methylcyclohexanol.

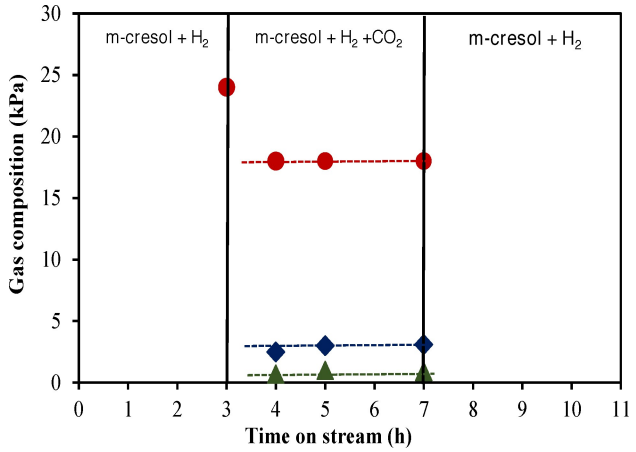

Figure 5. Evolution of gas composition during HDO of m-cresol (350 °C, 30 bar) performed in the presence of 24 KPa of CO_2 (●) CO_2; (◆) CH_4; (▲) CO.

catalyst surface leading to an irreversible deactivation, as observed in Figure 4c. In the literature, the effect of CO and CO_2 presence in HDO feed on the catalyst activity is poorly reported. For instance, Olcese et al.[12] investigated the effect of feeding CO, CO_2, CH_4 and H_2O during the HDO of guaiacol at 400 °C, under atmospheric pressure, using a Fe/SiO_2 catalyst. When reaction is conducted under pure H_2, guaiacol conversion decreases with reaction time, due to the Fe-catalyst deactivation. The authors reported that during the experiments carried out with CO_2, the deactivation is reduced in agreement with the results reported here. The presence of CO was reported to negatively impact the conversion rate, an effect that was ascribed to (i) carburization of iron; and (ii) coke accumulation, promoted by the CO dismutation reaction at the catalyst surface.

In order to verify the causes of catalyst deactivation, a possible sintering of metallic particles was verified by XRD analysis of the spent catalysts (Fig. S4, ESI) and the extent of coke formation during reaction was investigated by TPO analysis (Figure 6). From the XRD patterns it was observed diffraction lines in $2\theta = 44.5$, 52 and 76° associated to the Co^0 phase. The absence of additional lines excludes the oxidation of Co particles during reaction. The Co particle size, calculated by

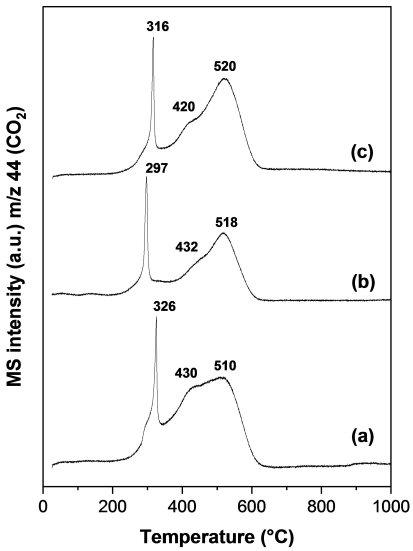

Figure 6. TPO profiles of the spent Co/SBA catalyst after HDO reaction of m-cresol carried out at 350 °C during 8 hours on stream under (a) H_2, (b) $H_2 + CO_2$; (c) $H_2 + CO$.

the Scherrer equation, was 8.7, 8.3 and 8.5 nm for the catalysts after reaction under only H_2, H_2+CO_2 and H_2+CO, respectively, thus indicating that sintering occurred during reaction. However, no difference is observed depending on the gas environment and thus we can suggest that sintering mainly occurs in the first hours of reaction, explaining the decrease in the hydrogenation activity with the yield of methylcyclohexane decreasing while increasing the yield of methylcyclohexenes. Regarding the TPO analysis, all profiles (in the presence of only H_2, and CO_2 or CO added to the H_2 feed) were almost similar. A narrow peak at around 326 °C and a broad double peak between 350–600 °C (the maximum of temperature located at 430 and 510 °C) are observed. The narrow peak at low temperature was attributed to the combustion of adsorbed reactant or reaction intermediates at the catalyst surface.[5f,24] The high temperature reaction is assigned to the combustion of coke.[19a,25] Small differences are observed in the intensity of the peaks: the intensity of the peak at around 430 °C decreases when reaction was conducted under CO_2 or CO added to the feed. Besides that, the loss of weight, determined by TGA analysis, was 0.091 g/g_{cat} (H_2), 0.052 g/g_{cat} (H_2+CO_2) and 0.075 g/g_{cat} (H_2+CO). The presence of CO_2 seems to slightly inhibit the formation of coke, explaining the better stability of the catalyst when CO_2 is introduced in the gas phase (Figure 3). A detailed investigation on the effect of CO_2 exposure in the catalyst surface will be realized soon. CO presence also seems to prevent coke deposition, but in a less extent. Therefore, under only H_2, the catalyst deactivation can be explained both by coke accumulation and metal sintering. The strong deactivation caused by the presence of CO is preferably ascribed to an irreversible adsorption of CO on the active sites, rather than to coke accumulation.

Computational results

In order to find the most stable configurations for the m-cresol, CO and CO_2 over both bare and supported silica surfaces, different interactions modes have been tested. Five possible interaction sites (isolated, geminal, vicinal, nest-1,nest-2) exist on the pure SiO_2-3.3 surface. These adsorption sites are described and discussed in previous studies.[13,26] For the metal supported catalysts, the molecules can adsorb either on the top of the metal cluster or at the cluster@surface interface. For each interaction mode, we have studied different orientations of the considered molecules and different positions at the interface or on the surface.

The model selected as cobalt cluster contains 13 atoms (size of 13 Å) since it is dynamically stable.[27] The determining factor of the stability of this structure is the bond symmetry, i.e., the presence of the maximum number of the nearest atoms.[27d] This cluster also exhibits a high dynamic stability which is characterized by significant degeneracy of the vibration amplitudes of the cluster. We have shown previously[28] that these clusters are energetically stable on the silica surface. The size of the cluster is considered sufficiently large to neglect the effect of the surface. When adsorbed on the cluster, the molecules are isolated from the surface (6 Å). Therefore, a cluster size will have a limited effect on the interaction mode of m-cresol, CO and CO_2 molecules

Table 3 shows the most stable PBE+U+D2 adsorption energies (kJ mol^{-1}) of m-cresol, CO and CO_2 on each adsorption site over bare and supported silica surfaces. The adsorption energy is given by Equation (1):

$$\Delta E = E_{sys} - E_{surf} - E_{mol} \quad (1)$$

where E_{sys}, E_{surf} and E_{mol} are the corresponding PBE+U+D2 total energies of the total system, the considered surfaces (bare silica and Co supported on silica), and the molecules (m-cresol, CO, CO_2), respectively. These energies are computed in the same supercell in order to minimize the numerical errors.

Over pure silica surface, m-cresol and CO prefer to occupy the nest-1 site with an interaction energy of −90 and −12 kJ mol^{-1}, respectively, while carbon dioxide prefers to accommodate on the nest-2 site, with an adsorption energy of −22 kJ mol^{-1}. Over silica supported Co_{13} cluster, results show that the adsorption of the m-cresol, CO, CO_2 molecules preferentially occur at the interface Co_{13}@SiO_2-3.3 with interaction energies of −214, −177, −101 kJ mol^{-1}, respectively, and the adsorption on the top of the Co_{13} cluster showing a ΔE of −194, −145, and −78 kJ mol^{-1}. These values suggest that in all cases, m-cresol is preferentially adsorbed and the adsorption of all molecules are more favorable at the interface cluster-silica than on the top of the metal cluster.

The most stable adsorption structures of m-cresol, CO and CO_2 on bare silica and silica supported Co surfaces are shown in Figure 7. Results show that m-cresol prefers to adsorb via a parallel adsorption mode onto the bare silica surface through its aromatic ring while making two hydrogen bonds with the nest-1 adsorption site of lengths 1.79 and 1.86 Å. The corresponding interaction energy to this adsorption mode is −90 kJ mol^{-1}. For the Co supported surface, the adsorption of m-cresol becomes stronger, reaching −214 kJ mol^{-1} at the interface Co_{13}@silica. In this case m-cresol interacts simulta-

Table 3. Computed PBE+U+D2 adsorption energies (kJ mol^{-1}) of m-cresol, CO and CO_2 molecules over bare silica surface and supported Co_{13} on silica surface (3.3 OH/m^2) through their most stable adsorption sites.

Inter mode	Silica Isolated	Geminal	Vicinal	Nest-1	Nest-2	Co_{13}/silica Cluster Co_{13}	Interface Co_{13}@SiO_2
m-cresol	−48	−33	−76	−90	−58	−194	−214
CO	−11	−11	−11	−12	−12	−145	−177
CO_2	−12	−16	−19	−19	−22	−78	−101

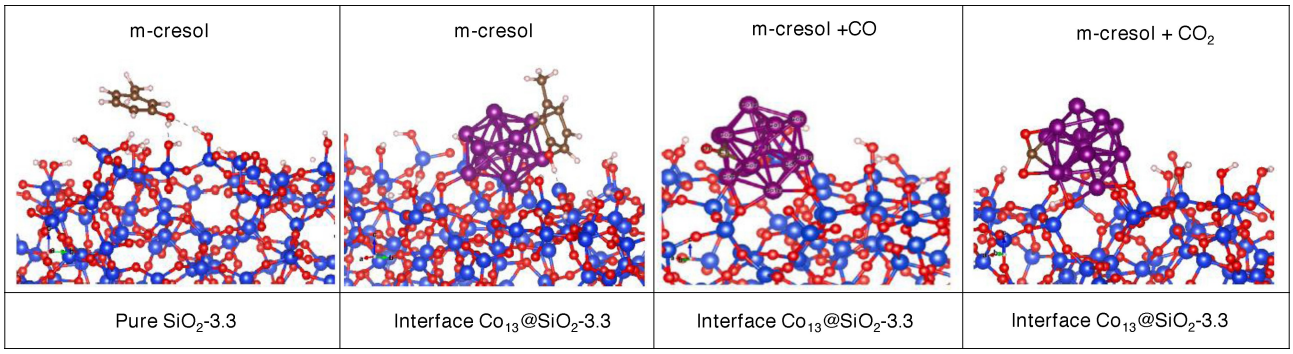

Figure 7. Most stable interactions of m-cresol, CO and CO_2 with silica surface and silica supported Co_{13} surfaces.

neously with the cobalt cluster and the silica surface through its aromatic ring via three C–Co bonds lengths ranging between 2.08 and 2.11 Å, while making another hydrogen bond of 1.75 Å between the hydroxyl group of the molecule and the silanol site of the silica surface. The adsorption of CO on the pure silica surface is not favorable (−11 or −12 kJ mol^{-1} on any silanol group). However, CO strongly interacts with the interface Co13@silica (−177 kJ mol^{-1}), through two C–Co bonds (bridge adsorption). The equilibrium C–Co distances were found to be between 1.8–2.09 Å. CO_2 also interacts weakly with the pure SiO_2-3.3 surface (E_{ads} = −12 kJ mol^{-1}), where the closed silanol site is found at 3.0 Å. We found that the C–O bond length of the CO_2 molecule is 1.18 Å and the angle is slightly modified (0.5°) compared to the isolated molecule. For the silica supported Co, CO_2 strongly adsorbs at the interface cluster@silica (E_{ads} = −101 kJ mol^{-1}) making two O–Co and two C–Co bonds with equilibrium distances of about 2.05 Å and (1.94, 2.18 Å), respectively.

The adsorption energies of the most favorable configurations of m-cresol and the inhibiting molecules (CO, CO_2) on silica surface and at the metal cluster-silica interface are gathered in Figure 8. Adsorption energies of all molecules on silica are significantly lower than on the Co-SiO_2 interface demonstrating that the molecules prefer to adsorb and react at the Co–SiO_2 interface. In this case, the ΔE_2 of m-cresol is 37 and 113 kJ mol^{-1} larger than those for CO and CO_2 molecules, respectively. This indicates that Co_{13}@SiO_2 interface is potentially more selective toward m-cresol adsorption rather than CO_2 and thus, no inhibiting effect of CO_2 is expected, as observed experimentally (Figure 3 and 4b). However, for CO, the difference is smaller, and thus m-cresol and CO will compete to adsorb on the catalyst surface. The competition between both oxygenated molecules (m-cresol and CO) can result in the decrease of active sites available for m-cresol adsorption and activation explaining the inhibiting effect of CO observed experimentally (Fig. 4c).

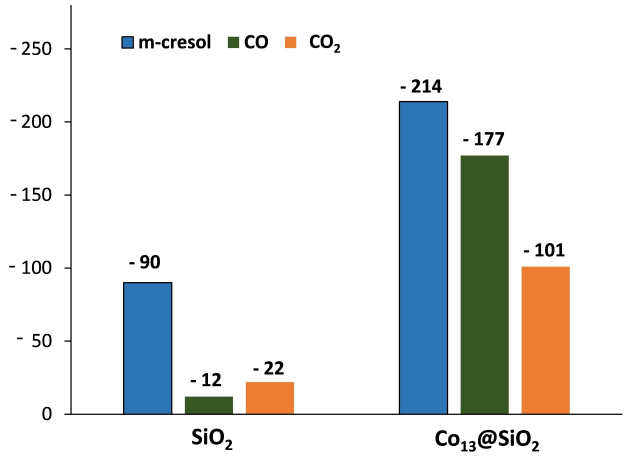

Figure 8. PBE + U + D2 computed ΔE_2 of the most favorable configurations of m-cresol, CO and CO_2 on pure silica and on the Co_{13}@SiO_2 interface.

Conclusion

In this work, Co nanoparticles were stabilized in the porosity of SBA-15 and evaluated for the HDO reaction of m-cresol at 350 °C and 30 bar of pressure. The catalyst presented a good selectivity toward deoxygenated products, products being mainly methylcyclohexenes and methylcyclohexane. However, a fast deactivation of the catalyst was observed, which was attributed to coke accumulation. For a better understanding of the m-cresol HDO under pyrolysis gas conditions, the effect of co-feeding CO or CO_2 was investigated. Results showed that CO_2 has a positive effect on m-cresol HDO reaction, reducing catalyst deactivation. On the opposite, CO had a significant negative effect. Strong decrease in m-cresol conversion is observed when CO is added to the stream, and the deactivation is observed to be irreversible. Experimental results suggest that the effect of CO can be attributed to a competitive adsorption between CO and m-cresol, with CO remaining adsorbed on catalyst surface rather than forming coke. DFT calculations confirm that m-cresol adsorbs preferentially on the Co_{13}@silica interface, rather on the silica surface. Adsorption energy of CO_2 is much lower compared to that of m-cresol, showing that the inhibitory effect of CO_2 could be considered as negligible. On the contrary, comparable adsorption energies are observed for CO and m-cresol then confirming the potential competitive

adsorption between both molecules on the catalyst surface during reaction, which can be the initial step of the catalyst deactivation experimentally observed. Finally, our findings may open a new way to activate the catalyst (in the presence of CO_2) to avoid deactivation, which is a big issue in the development of HDO catalysts.

Experimental Section

Support preparation. Mesoporous SBA-15 silica was used as support for the preparation of supported cobalt catalyst. The triblock copolymer (4 g of Pluronic P123, M = 5800), used as structure directing agent, was solubilized at 40 °C under continuous stirring in 150 mL of 1.6 M HCl solution.[29] The silicon precursor (TEOS 98 wt.%) was added dropwise in order to assure a slow condensation rate while the synthesis temperature was maintained at 40 °C for 24 h under high stirring rate. In order to obtain a homogenous distribution of mesopore, a hydrothermal treatment was realized in a Teflon-lied autoclave at 100 °C for 48 h. Afterward, the SBA-15 was recovered by filtration, intensively washed with deionized water and dried at 100 °C overnight. In this work, for the melt-infiltration method utilized for the preparation of the silica supported-Co catalyst, the SBA-15 was not calcined.

Catalyst preparation. For the dispersion of cobalt within SBA-15 porosity, we used the melt infiltration in intrawall porosity (MI-IWP) method.[14] First, the nitrate precursor (0.007 mole of $Co(NO_3)_2\ 6H_2O$, 98 wt.%, amount needed to obtain 10 wt.% of cobalt loading in the silica) was mixed with uncalcined SBA-15. After a gentle hand grinding until a homogenous powder be obtained,[14a] the powder was transferred into a PTFE autoclave and a thermal treatment was done at the melting point of the precursor (57 °C) during 4 days. The CoO_x supported phase onto SBA-15 was obtained by calcination at 500 °C for 6 h (heating ramp of 1.5 °C min^{-1}) and then reduced at 800 °C (heating ramp of 5 °C min^{-1}) for 1 h under 50 mL min^{-1} of pure hydrogen. The calcined catalyst was designated as CoOx/SBA and after reduction as Co/SBA.

A Co/SiO_2 catalyst was prepared for comparison. A commercial silica (Hi-Sil 915, PPG industries) was used as a support. The catalyst was prepared by wetness incipient impregnation of the support using an aqueous solution of $Co(NO_3)_2.6H_2O$ in order to obtain 10 wt;% of Co. After impregnation, the solid was dried overnight at 120 °C and then calcined at 500 °C for 3 h, 1.5 °C min^{-1}.

Catalyst characterization. For determination of the textural properties of the materials, adsorption/desorption N_2 physisorption at −196 °C was performed using a Micromeritics Tristar II automated gas sorption system. Before analysis, 50 mg of calcined sample was outgassed under dynamic vacuum at 300 °C for 3 h. Specific surface area was determined using the multipoint B.E.T. algorithm, in the 0.10–0.25 P/P_0 interval. The pore size distribution was determined using the B.J.H. method from the desorption branch of the isotherm. Pore volume was measured at $P/P_0 = 0.98$ on the desorption branch.

Identification of crystalline phase was performed by X-ray diffraction (XRD) analysis, using a Bruker X-ray AXS D8 Advance diffractometer in Bragg-Brentano geometry configuration fitted with a LynxEye Super Speed detector. The diffractogram was recorded with Cu Kα radiation (λ = 0.154 nm, 40 kV, 30 mA) in the 10–80° 2θ range with a 0.02° 2θ step.

The reducibility of the catalyst was studied by H_2-temperature programmed reduction (H_2-TPR). The analysis was performed on a Micromeritics AutoChem 2910 equipment, performing reduction from room temperature up to 1000 °C, applying a heating rate of 10 °C min^{-1}, under 10 vol.% of H_2 in Ar flow (flow rate of 30 mL min^{-1}). Prior to the TPR run, the samples were pre-treated under pure oxygen (30 mL min^{-1}) at 400 °C during 1 h. During experiment, hydrogen consumption was monitored using a TCD detector.

Material morphology and distribution of Co particles were studied by scanning transmission electron microscopy (S/TEM) using high angle annular dark field (HAADF) detector. The analysis was performed on a TITAN Themis 300 S/TEM instrument, with a probe aberration corrector and monochromator, spatial resolution of 70 pm and energy resolution of 150 meV. The microscope is equipped with a super-X windowless 4 quadrant SDD (silicon drift detector) detection system for the STEM-EDX (energy dispersive x-ray) mapping. The experiments were performed with a 0.5 nm probe size, a convergence angle of 21 mrad and a probe current of approximately 100 pA. For the HAADF images, collection angles were between 50 and 200 mrad. Prior to observation, the sample was reduced at 800 °C (5 °C min^{-1}) during 1 h under pure H_2 flow. After the reduction step, the sample was embedded in a polymeric Epoxy resin and cut into sections of 50 nm using an ultramicrotome equipped with a diamond knife. Cuts were deposited on carbon grids for analysis. The Co nanoparticles sizes were measured using ImageJ.

Catalyst acidity was measured by DRIFTS using adsorbed pyridine as a probe molecule. The experiment was performed on a Nicolet Nexus instrument equipped with a DTGS detector and a quartz cell with CaF_2 windows. The Co/SBA sample was initially reduced *ex situ* in the same conditions than those used for the catalytic reaction (800 °C, 5 °C min^{-1} reduction performed under 50 mL min^{-1} of pure H_2 during 1 h). After reduction, the sample was heated at 400 °C under vacuum for 12 h. Then, the sample was cooled down to 150 °C, and a spectrum of the sample was registered as reference. After that, pyridine adsorption was carried out during 5 min, and then a vacuum purge was performed during 1 h. Finally, spectra were recorded after heating under vacuum at 150 °C. Additional spectra were recorded between 150 and 450 °C at a resolution of 2 cm^{-1} and accumulating 64 scans.

Transformation of m-cresol. The catalytic transformation of m-cresol was performed in a down flow tubular inox fixed-bed reactor operating at 350 °C and 30 bar of total pressure. The catalyst was previously reduced *ex situ* at 800 °C (5 °C min^{-1}) during 1 h under pure H_2 flow rate (50 mL min^{-1}). After reduction step, the catalyst was cooled under H_2 and it was transferred to the HDO reactor. Before reaction, the catalyst was still subjected to treatment under pure hydrogen (4.7 NL h^{-1}) at 350 °C for 1 h, under 30 bar of total pressure. Then, the flow of hydrogen and the m-cresol feedstock were adjusted at different contact times, which were estimated by the W/F ratio, in order to obtain different levels of m-cresol conversion. The liquid feedstock, introduced at the top of the reactor by using a HPLC Gilson pump, was composed by m-cresol (7 mol%), decane (3 mol%) used as internal standard, and n-heptane as solvent. The H_2/m-cresol molar ratio was set to 60. In order to study the effect of co-feeding CO and CO_2 in the reaction flow, experiments were conducted with 24.26 bar of H_2, 0.39 bar of m-cresol and 0.24 bar of CO or CO_2 (given 2426, 39 and 24 kPa respectively).

The line at the bottom of the reactor was maintained at 10 °C using a Minichiller-Huber condenser. Thus, liquid samples were collected at selected reaction time and analyzed by a Varian 430 chromatograph equipped with a DB-5 capillary column (length 30 m; internal diameter: 0.25 mm, film thickness: 5 μm) and a flame-ionization detector (FID) for organics quantification. Gaseous reactants and/or products were analyzed by a Varian 450 chromatograph equipped

with a thermal conductivity detector (TCD) and three capillary columns: HayeSep T, HayeSep Q and one molecular sieve 13x (both of three with length of 0.5 m, inside diameter of 1/8 in and film thickness of 2 mm). The conversion of m-cresol and product selectivity were calculated using Equation (2) and (3):

$$\mathbf{X}\ (\mathbf{in}\ \%) = \frac{\mathbf{n^0}_{\mathbf{m-cresol}} - \mathbf{n}_{\mathbf{m-cresol}}}{\mathbf{n^0}_{\mathbf{m-cresol}}} \times 100 \quad (2)$$

$$\boldsymbol{S_i}\ (\mathbf{in\ mol}\ \%) = \frac{\mathbf{n_i}}{\mathbf{n^0}_{\mathbf{m-cresol}} - \mathbf{n}_{\mathbf{m-cresol}}} \times 100 \quad (3)$$

Where $n^0_{m\text{-}cresol}$ and $n_{m\text{-}cresol}$ are the mole quantity of m-cresol in the feedstock and in the collected samples respectively; n_i is the mole quantity of a given *i* product.

The total reaction rate (r_{TOT}, mmol g^{-1} h^{-1}) and the reaction rates for each pathway (r_{DDO} for deoxygenation leading to toluene; r_{HYD} for aromatic ring hydrogenation mainly leading to 3-methylcyclohexanone, methylcyclohexene isomers and methylcyclohexane) were calculated considering the conversion of m-cresol and the yield of the respective products (Yi) using Equation (4) and (5), assuming a first order reaction rate:

$$\mathbf{r_{TOT}}\ (\mathbf{in\ mmol}\ \boldsymbol{g}^{-1}\ \mathbf{h}^{-1}) = -\frac{\boldsymbol{F}}{\boldsymbol{W}}\boldsymbol{Ln}\ (1-\boldsymbol{X}) \quad (4)$$

$$\mathbf{r_y}\ (\mathbf{in\ mmol}\ \boldsymbol{g}^{-1}\ \mathbf{h}^{-1}) = \boldsymbol{r_{TOT}}.\ \boldsymbol{S_y} \quad (5)$$

where r_{TOT} is the total reaction rate for m-cresol transformation, r_y is the reaction rate for reaction route y (DDO, HYD), X is the m-cresol conversion, F is the m-cresol flow rate (mmol h^{-1}), W is the catalyst weight (g) and S_y is the selectivity product y (toluene for DDO route, 3-methylcyclohexanone, 3-methylcylohexanol, methylcyclohexene isomers and methylcyclohexane for the HYD route).

DFT Calculations. Calculations are conducted using the Vienna Ab Initio Simulation Package (VASP version 5.4)[30] based on the projector augmented wave method (PAW).[31] Systematically periodic spin polarized density functional theory calculations were performed in order to find the most stable adsorption structures of the target compounds. Perdew, Burk and Ernzerhof (PBE) formulation of the generalized gradient approximation for the exchange-correlation potential was used together with the Grimme D2 dispersion correction to account for van der Waals interactions.[32] The Hubbard U and J parameters[33] (fixed to 3.0 and 0.9 eV, respectively[28]) were included in order to take into account the strong d electron-electron interaction on the cobalt nanoparticles

In this work, we considered silica surface with a silanol density of 3.3 OH/nm^2, which corresponds to what was determined for mesoporous silica type materials. This surface has been constructed by Comas-Vives[34] via dehydroxylation process of the fully hydroxylated silica surface using a periodic supercell of 375 atoms. 13 atoms were used to model the supported cobalt clusters, which adopts the D_{3d} symmetry.[33] For both pure and supported silica systems, 20 Å of vacuum was added to separate the periodically repeated slabs along the z direction. For all calculations, only the Γ point was used for the integration of the first Brillouin zone due to the large size of the considered systems. The total energy difference was fixed to 10^{-6} eV for the convergence criterion, while the force criterion was set to 0.03 eV/Å. For the structure optimization, the positions of the title compounds, the Co_{13} cluster, and the first surface layer were relaxed, while those of the other layers are fixed.

Acknowledgements

This work (Pyreodeox project) was financially supported by ANR (Agence Nationale de la Recherche). Camila A. Teles and Frederic Richard acknowledge the financial support from the European Union (ERDF), "Region Nouvelle Aquitaine", and CAPES-COFECUB program (88881.142911/2017-01). The Chevreul Institute is acknowledged for its help in the development of this work through the ARCHI-CM project supported by the "Ministère de l'Enseignement Supérieur de la Recherche et de l'Innovation", the region "Hauts-de-France", the ERDF program of the European Union and the "Métropole Européenne de Lille". Saber Gueddida, Sebastien Lebègue and Michael Badawi acknowledge financial support through the COMETE, France project (COnception in silico de Matériaux pour l'EnvironmenT et l'Energie) cofounded by the European Union under the program "FEDER-FSE Lorraine et Massif des Vosges 2014–2020)".

Conflict of Interest

The authors declare no conflict of interest.

Data Availability Statement

The data that support the findings of this study are available from the corresponding author upon reasonable request.

Keywords: HDO · m-cresol · inhibiting effect · carbon monoxide · carbon dioxide · cobalt · SBA-15

[1] a) Y. Cao, S. S. Chen, S. Zhang, Y. S. Ok, B. M. Matsagar, K. C-W. Wu, D. C. W. Tsang, *Bioresour. Technol.* **2019**, *291*, 121878; b) S. Sethupathy, G. Murillo Morales, L. Gao, H. Wang, B. Yang, J. Jiang, J. Sun, D. Zhu, *Bioresour. Technol.* **2022**, *347*, 126696; c) S. S. Wong, R. Shu, J. Zhang, H. Liu, N. Yan, *Chem. Soc. Rev.* **2020**, *49 (15)*, 5510–5560.
[2] A. Kumar, Anushree, J. Kumar, T. Bhaskar, *J. Energy Inst.* **2020**, *93 (1)*, 235–271.
[3] R. Shu, R. Li, B. Lin, C. Wang, Z. Cheng, Y. Chen, *Biomass Bioenergy* **2020**, *132*, 105432.
[4] a) A. N. Kay Lup, F. Abnisa, W. M. A. W. Daud, M. K. Aroua, *Appl. Catal. A* **2017**, *541*, 87–106; b) V. O. O. Gonçalves, S. Brunet, F. Richard, *Catal. Lett.* **2016**, *146 (8)*, 1562–1573; c) Q. Tan, G. Wang, L. Nie, A. Dinse, C. Buda, J. Shabaker, D. E. Resasco, *ACS Catal.* **2015**, *5 (11)*, 6271–6283.
[5] a) L. Nie, D. E. Resasco, *J. Catal.* **2014**, *317*, 22–29; b) P. M. de-Souza, L. Nie, L. E. P. Borges, F. B. Noronha, D. E. Resasco, *Catal. Lett.* **2014**, *144 (12)*, 2005–2011; c) M. B. Griffin, G. A. Ferguson, D. A. Ruddy, M. J. Biddy, G. T. Beckham, J. A. Schaidle, *ACS Catal.* **2016**, *6 (4)*, 2715–2727; d) V. O. O. Gonçalves, C. Ciotonea, S. Arrii-Clacens, N. Guignard, C. Roudaut, J. Rousseau, J–M. Clacens, S. Royer, F. Richard, *Appl. Catal. B* **2017**, *214*, 57–66; e) F. Yang, D. Liu, H. Wang, X. Liu, J. Han, Q. Ge, X. Zhu, *J. Catal.* **2017**, *349*, 84–97; f) C. A. Teles, P. M. de-Souza, R. C. Rabelo-Neto, M. B. Griffin, C. Mukarakate, K. A. Orton, D. E. Resasco, F. B. Noronha, *Appl. Catal. B* **2018**, *238*, 38–50.
[6] a) L. Nie, P. M. de Souza, F. B. Noronha, W. An, T. Sooknoi, D. E. Resasco, *J. Mol. Catal. A* **2014**, *388–389*, 47–55; b) F. Yang, H. Wang, J. Han, Q. Ge, X. Zhu, *Catal. Today* **2019**, *330*, 149–156; c) X. Liu, W. An, C. H. Turner, D. E. Resasco, *J. Catal.* **2018**, *359*, 272–286; d) V. O. O. Gonçalves, W. H. S. M. Talon, V. Kartnaller, F. Venancio, J. Cajaiba, T. Cabioc'h, J–M. Clacens, F. Richard, *Catal. Today* **2021**, *377*, 135–144.
[7] F. Yang, D. Liu, Y. Zhao, H. Wang, J. Han, Q. Ge, X. Zhu, *ACS Catal.* **2018**, *8 (3)*, 1672–1682.

[8] D. Liu, G. Li, F. Yang, H. Wang, J. Han, X. Zhu, Q. Ge, *J. Phys. Chem. C* **2017**, *121 (22)*, 12249–12260.
[9] a) M. B. Figueirêdo, I. Hita, P. J. Deuss, R. H. Venderbosch, H. J. Heeres, *Green Chem.* **2022**, *24 (12)*, 4680–4702; b) W. Li, N. Wanninayake, X. Gao, M. Li, Y. Pu, D–Y. Kim, A. J. Ragauskas, J. Shi, *ACS Sustainable Chem. Eng.* **2020**, *8 (42)*, 15843–15854.
[10] C. Bouvier, Y, Romero, F. Richard, S. Brunet, *Green Chem.* **2011**, *13*, 2441–2451.
[11] M. Badawi, J–F. Paul, S. Cristol, E. Payen, *Catal. Commun.* **2011**, *12 (10)*, 901–905.
[12] R. Olcese, M. M. Bettahar, B. Malaman, J. Ghanbaja, L. Tibavizco, D. Petitjean, A. Dufour, *Appl. Catal. B* **2013**, *129*, 528–538.
[13] S. Gueddida, S. Lebègue, A. Pasc, A. Dufour, M. Badawi, *Appl. Surf. Sci.* **2021**, *567*, 150790.
[14] a) C. Ciotonea, B. Dragoi, A. Ungureanu, C. Catrinescu, S. Petit, H. Alamdari, E. Marceau, E. Dumitriu, S. Royer, *Catal. Sci. Technol.* **2017**, *7 (22)*, 5448–5456; b) S. Chen, C. Ciotonea, A. Ungureanu, E. Dumitriu, C. Catrinescu, R. Wojcieszak, F. Dumeignil, S. Royer, *Catal. Today* **2019**, *334*, 48–58.
[15] C. Ciotonea, B. Dragoi, A. Ungureanu, A. Chirieac, S. Petit, S. Royer, E. Dumitriu, *Chem. Commun.* **2013**, *49 (69)*, 7665.
[16] C. A. Teles, P. M. de-Souza, R. C. Rabelo-Neto, A. Teran, G. Jacobs, D. E. Resasco, F. B. Noronha, *ACS Sustainable Chem. Eng.* **2021**, *9 (38)*, 12870–12884.
[17] C. Chen, G. Chen, F. Yang, H. Wang, J. Han, Q. Ge, X. Zhu, *Chem. Eng. Sci.* **2015**, *135*, 145–154.
[18] C. A. Teles, R. C. Rabelo-Neto, J. R. de Lima, L. V. Mattos, D. E. Resasco, F. B. Noronha, *Catal. Lett.* **2016**, *146 (10)*, 1848–1857.
[19] a) F. Yang, H. Wang, J. Han, Q. Ge, X. Zhu, *Catal. Today* **2020**, *347*, 79–86; b) P–J. Hsu, J–W. Jiang, Y–C. Lin, *ACS Sustainable Chem. Eng.* **2018**, *6 (1)*, 660–667.
[20] V. O. O. Gonçalves, P. M. de Souza, T. Cabioc'h, V. T. da Silva, F. B. Noronha, F. Richard, *Appl. Catal. B* **2017**, *219*, 619–628.
[21] P. M. De-Souza, L. Nie, L. E. P. Borges, F. B. Noronha, D. E. Resasco, *Catal. Let.* **2014**, *144*, 2005–2011.
[22] C. A. Teles, L. R. Francisco, V. O. O. Gonçalves, F. B. Noronha, F. Richard, *Catal. Lett.* **2022**, doi: 10.1007/s10562-022-04171-4.
[23] a) P. M. de Souza, R. C. Rabelo-Neto, L. E. P. Borges, G. Jacobs, B. H. Davis, D. E. Resasco, F. B. Noronha, *ACS Catal.* **2017**, *7 (3)*, 2058–2073; b) C. A. Teles, R. C. Rabelo-Neto, G. Jacobs, B. H. Davis, D. E. Resasco, F. B. Noronha, *ChemCatChem* **2017**, *9 (14)*, 2850–2863; c) M. Shetty, K. Murugappan, T. Prasomsri, W. H. Green, Y. Román-Leshkov, *J. Catal.* **2015**, *331*, 86–97.
[24] C. A. Teles, R. C. Rabelo-Neto, N. Duong, J. Quiroz, P. H. C. Camargo, G. Jacobs, D. E. Resasco, F. B. Noronha, *Appl. Catal. B* **2020**, *277*, 119238.
[25] X. Zhu, L. Nie, L. L. Lobban, R. G. Mallinson, D. E. Resasco, *Energy Fuels* **2014**, *28 (6)*, 4104–4111.
[26] a) S. Gueddida, S. Lebègue, M. Badawi, *J. Phys. Chem. C* **2020**, *124*, 20262; b) S. Gueddida, M. Badawi, T. Aminabhavi, S. Lebègue, *Mol. Syst. Des. Eng.* **2021**, *6*, 817.
[27] a) W. Hu, L. Mei, H. Li, *Solid State Commun.* **1996**, *100*, 129–131; b) M. Kabir, A. Mookerjee, A. K. Bhattacharya, *Phys. Rev. A* **2004**, *69*, 043203; c) Z. Xie, Q.-M. Ma, Y. Liu, Y.-C. Li, *Phys. Lett. A* **2005**, *342*, 459–467; d) G. R. S. D. Borisova, E. Chulkov, *Phys. Solid State* **2010**, *52*, 838–843.
[28] S. Gueddida, S. Lebègue, M. Badawi, *Appl. Surf. Sci.* **2020**, *533*, 147422.
[29] A. Ungureanu, B. Dragoi, V. Hulea, T. Cacciaguerra, D. Meloni, V. Solinas, E. Dumitriu, *Microporous Mesoporous Mater.* **2012**, *163*, 51–64.
[30] G. Kresse, J. Furthmuller, *Phys. Rev. B* **1996**, *54*, 11169.
[31] P. E. Blochl, *Phys. Rev. B* **1994**, *50*, 17953.
[32] a) S. Grimme, *J. Comput. Chem.* **2006**, *27*, 1787; b) T. Bucko, J. Hafner, S. Lebègue, J. G. Angyan, *J. Phys. Chem. A* **2010**, *114*, 11814.
[33] O. Bengone, M. Alouani, P. Blochl, J. Hugel, *Phys. Rev. B* **2000**, *62*, 16392.
[34] A. Comas-Vives, *Phys. Chem. Chem. Phys.* **2016**, *18*, 7475.

Manuscript received: October 31, 2022
Revised manuscript received: January 25, 2023
Version of record online: March 8, 2023